HHS Public Access

Author manuscript

ACS Chem Biol. Author manuscript; available in PMC 2019 June 15.

Published in final edited form as:

ACS Chem Biol. 2018 June 15; 13(6): 1560–1568. doi:10.1021/acschembio.8b00157.

Temporal profiling establishes a dynamic *S*-palmitoylation cycle

Sang Joon Won[1] and **Brent R. Martin**[1,2,*]

[1]Program in Chemical Biology, University of Michigan, 930 N. University Ave., Ann Arbor, MI 48109, USA

[2]Department of Chemistry, University of Michigan, 930 N. University Ave., Ann Arbor, MI 48109, USA

Abstract

S-palmitoylation is required for membrane anchoring, proper trafficking, and the normal function of hundreds of integral and peripheral membrane proteins. Previous bioorthogonal pulse-chase proteomics analyses identified Ras family GTPases, polarity proteins, and G proteins as rapidly cycling *S*-palmitoylated proteins sensitive to depalmitoylase inhibition, yet the breadth of enzyme regulated dynamic *S*-palmitoylation largely remains a mystery. Here we present a pulsed bioorthogonal *S*-palmitoylation assay for temporal analysis of *S*-palmitoylation dynamics. Low concentration hexadecylfluorophosphonate (HDFP) inactivates the APT and ABHD17 families of depalmitoylases, which dramatically increases alkynyl-fatty acid labeling and stratifies *S*-palmitoylated proteins into kinetically distinct subgroups. Most surprisingly, HDFP treatment does not affect steady-state *S*-palmitoylation levels, despite inhibiting all validated depalmitoylating enzymes. *S*-palmitoylation profiling of APT1$^{-/-}$/APT2$^{-/-}$ mouse brains similarly show no change in *S*-palmitoylation levels. In comparison with hydroxylamine-switch methods, bioorthogonal alkynyl fatty acids are only incorporated into a small fraction of dynamic *S*-palmitoylated proteins, raising the possibility that *S*-palmitoylation is more stable than generally characterized. Overall, disrupting depalmitoylase activity enhances alkynyl fatty acid incorporation, but does not greatly affect steady state *S*-palmitoylation across the proteome.

Introduction

The palmitoylation / depalmitoylation machinery establishes a spatially directed flow of *S*-palmitoylated proteins along vesicular pathways towards the plasma membrane, effectively overriding entropy-driven random membrane distribution[1]. The complete cycle occurs within seconds, where proteins are dynamically palmitoylated and depalmitoylated to effectively restrict transport along the flux of vesicular traffic[2]. Generic depalmitoylase inhibition blocks this cycle, distributing plasma membrane targeted peripheral membrane proteins, such as Ras-family small GTPases[3] and G-proteins[4], randomly across internal membranes. In contrast, inhibition of the depalmitoylase APT2 corrects an imbalanced palmitoylation cycle in malignant cells to restore lateral membrane localization of the multi-

*Correspondence: brentrm@umich.edu.

Author Contributions

S.J.W. performed all experiments. S.J.W and B.R.M designed all experiments and wrote the manuscript.

domain polarity scaffolding protein SCRIB[5]. Across decades of study, protein depalmitoylation has emerged as a critical mechanism for dynamic membrane localization, trafficking, and functional regulation, yet the breadth of substrates and global dynamics remain poorly characterized on a global scale[6].

The recent development bioorthogonal labeling strategies has transformed the analysis of dynamic *S*-palmitoylation[7]. Pulse-chase metabolic labeling with the alkynyl-fatty acid reporter 17-octadecynoic acid (17-ODYA) and click chemistry conjugation to biotin-azide has enabled quantitative proteomics assignment of proteins with accelerated turnover dynamics, including Ras-family small GTPases, G-proteins, and cell polarity organizing proteins[8]. This accelerated turnover is stabilized by treatment with hexadecylfluorophosphonate (HDFP), a broad inhibitor of cellular lipases[8]. While this approach identified new targets of depalmitoylase regulation, the reported limited profile falls short of many historical biochemical analyses demonstrating widespread depalmitoylase action across *S*-palmitoylated substrates[6]. This discrepancy is likely due to the poor sensitivity of the alkynyl-fatty acid pulse-chase assay, particularly since alkynyl fatty acids are incorporated broadly across lipid classes[9]. Once distributed across membrane lipids, addition of excess palmitate is not very efficient in pulse-chase experiments and limits sensitive analysis of proteome-wide *S*-palmitoylation turnover rates.

To address these technical challenges, we now present a multiplexed pulse-labeling method for profiling the kinetics of alkynyl fatty acid incorporation. The resulting kinetic signatures corroborate previous pulse-chase analysis and reveal the presence of a conserved *S*-palmitoylation kinetic profile between different cell lines. In addition, HDFP increases alkynyl fatty acid incorporation through covalent inactivation of lipid hydrolase and depalmitoylase enzymes, revealing a much broader role for depalmitoylase regulation. While metabolic labeling highlights significant dynamics, hydroxylamine-switch methods fail to report any major steady-state *S*-palmitoylation changes. Accordingly, we propose metabolic labeling only accesses a dynamic fraction of modified proteins, and changes are largely lost in bulk steady-state analyses.

Results

In order to bypass the challenges inherent to pulse-chase analysis, we focused on profiling the overall palmitoylation flux across the proteome as a correlate to the rate of *S*-palmitoylation cycling. Interestingly, treatment with the promiscuous lipase inhibitor HDFP stimulates a time-dependent increase in alkynyl fatty acid incorporation broadly across labeled proteins, even at relatively early time points across multiple cell lines (Figures 1a, S1a, and S1b). HDFP increases 17-ODYA labeling by about 60% by in-gel fluorescence analysis. This effect is independent of the 17-ODYA labeling concentrations (Figure 1b) and is measureable at sub-micromolar HDFP concentrations. Competitive activity-based protein profiling (ABPP) with fluorophosphonate-rhodamine (FP-TAMRA) confirmed inactivation of the depalmitoylase enzymes APT1 and APT2 at sub-micromolar HDFP concentrations sufficient to stimulate 17-ODYA incorporation (Figures 1c and 1d). Selective APT1, APT2, and/or PPT1 inhibition had no significant effect on 17-ODYA incorporation, suggesting the enhanced labeling requires inhibition of alternative HDFP-sensitive hydrolases (Figure 1e,

Figures S2a-b). More sensitive mass spectrometry analysis identified a subset of privileged HDFP targets (Figure 1f **and** Table S1) including fatty acid synthase (FASN), APT1, APT2, and ABHD17 family depalmitoylase enzymes. Selective inhibitors of FASN, PPT1, ABHD6, CES3, and NCEH1 similarly failed to stimulate 17-ODYA incorporation (Figures S2c-f). Since FASN inhibition has no effect on 17-ODYA incorporation, the HDFP effect is unlikely the consequence of a metabolic shift to a greater dependence on exogenous (alkynyl) fatty acids. While HDFP may be promiscuous across several lipases, it remains a potent modulator of *S*-palmitoylation useful for broadly profiling dynamic regulation.

Based on these observations, we designed a multiplexed mass spectrometry approach for temporal profiling of bioorthogonal *S*-palmitoylation (Figure 2a **and** Figure S3a). Human 293T cells were incubated with either palmitic acid or 17-ODYA for increasing lengths of time and harvested for biochemical analysis. After click chemistry conjugation to biotin-azide, streptavidin enrichment, and trypsin digestion, the eluted peptides were incubated with amine-reactive 6Plex-TMT isobaric labeling reagents and combined for quantitative mass spectrometry analysis. MultiNotch MS3 acquisition was used to limit ion interference and enhance the accuracy and precision of each measurement across the single 3 hr gradient[10]. Data was filtered based to include proteins annotation by at least 3 peptide spectrum matches (PSMs) and with >2-fold enrichment over the palmitic acid control across the last 3 time points. This analysis yielded several hundred specifically enriched proteins in 293T cells (Table S2), and nearly twice as many in haploid HAP1 cells chosen due to their emerging use in several *S*-palmitoylation studies[11, 12] (Table S3). This differential enrichment reflects either the intrinsic capacity of each cell line to metabolize exogenous fatty acids or represents competition between endogenous free fatty acid and exogenous alkynyl fatty acids. Enriched proteins were largely overlapping with previously published *S*-palmitoylation proteomics studies[13] (annotated in Tables S2 and S3).

Hierarchical cluster analysis classified *S*-palmitoylated proteins with different kinetic features. For example, NRAS, SCRIB, MTDH, and GNAS were all grouped together in the most rapidly *S*-palmitoylated sub-group (Figure S3b and Table S2), which directly correlates with reported pulse-chase studies[8]. Based on this analysis, proteins with rapid 17-ODYA labeling kinetics represent proteins regulated by an accelerated palmitoylation cycle (depalmitoylation and re-palmitoylation). Within this accelerated group, 17-ODYA incorporation peaks quickly followed by slow decay to a steady state equilibrium. Since this analysis relies on quantitation of tryptic peptides outside of the specific *S*-palmitoylation sites, proteins with multiple *S*-palmitoylation sites would predictably incorporate 17-ODYA at a faster rate than proteins with a single *S*-palmitoylation site. Despite this prediction, there is no clear correlation between multiply *S*-palmitoylated proteins and the rate of probe incorporation. For example, SNAP23 has at least 5 *S*-palmitoylation sites[14], yet demonstrates relatively average probe incorporation kinetics. While some sites may be more dynamic than others, the initial acquisition of the probe is not especially accelerated, suggesting multiply *S*-palmitoylated proteins (like SNAP23) may be more resistant to depalmitoylases.

In the same multiplexed analyses, HDFP treatment accelerated the kinetics of 17-ODYA labeling, defining different *S*-palmitoylated proteins with more or less sensitivity to

depalmitoylase inhibition (Figure 2b, Figure S3c, Tables S2–S3). Paired clustering of control and HDFP treated cells led to further kinetic segregation, stratifying proteins across 4 categories (Figures 2b-c **and** Figure S3c-d). Across the dataset, *S*-palmitoylated proteins are more efficiently labeled with 17-ODYA following HDFP treatment, which reflects both the effect of depalmitoylase inhibition and the relative rate of 17-ODYA incorporation back onto *S*-palmitoylated proteins by zDHHC protein acyl transferases. Thus, any increase in 17-ODYA incorporation also reflects differential rates of zDHHC enzyme catalyzed *S*-palmitoylation of their respective substrates. In addition, the observed slow decay likely reflects *de novo* depalmitoylase protein synthesis following HDFP hydrolysis, leading to fractional rescue of depalmitoylase activity in the later time points. Alternatively, other HDFP-insensitive hydrolases could slowly compensate, leading to the observed gradual decrease in labeling. This decrease is unlikely the consequence of proteolysis since low concentration HDFP does not inhibit any annotated proteases of peptidases (Figure 1f).

By hierarchical cluster analysis, Cluster 1 represents enriched proteins with both fast incorporation and relatively high sensitivity to HDFP at all time points (NRAS, MTDH, etc.). These proteins are robust targets of depalmitoylases, and demonstrate long-lasting changes throughout the time course. Cluster 1 most closely correlates with previous pulse-chase analysis of rapidly cycling *S*-palmitoylated proteins[8]. Cluster 2 represents enriched proteins with mild sensitivity to HDFP during the early to middle time points (RHOA, SNAP23, etc.). Cluster 3 represents enriched proteins with high HDFP sensitivity in early time points (SCRIB, FLOT2, etc.). Cluster 4 includes proteins with reduced labeling upon HDFP addition, and includes many proteins reported across multiple *S*-palmitoylation proteomics datasets[13]. These proteins may represent common false positives or could be enriched via chemically distinct mechanisms of protein acylation. In many instances, HDFP shifts proteins to a hyper *S*-palmitoylated state (MTDH, GNAS, SLC38A1, etc.), presumably by increasing the steady-state stoichiometry of probe incorporation. This observation is somewhat counterintuitive, since depalmitoylase inhibition would be predicted to trap proteins in their *S*-palmitoylated state, and not enhance 17-ODYA labeling. Since HDFP is a non-selective lipase inhibitor, any enhancement in *S*-palmitoylation could also be linked to increased 17-octadecynyl-CoA levels, which could synergize with depalmitoylase inhibition to enhance probe incorporation. Nonetheless, the kinetic clusters are largely similar between 293T cells and HAP1 cells, supporting a conserved program of temporal and enzymatic regulation (Figure 2d). Overall, the functional relevance of the observed stratification requires further analysis, especially since the data represents complicated network of zDHHC acyl transferases, depalmitoylases, and lipid processing enzymes.

Since HDFP promotes greater 17-ODYA labeling, we questioned whether this translates to an increase in steady-state *S*-palmitoylation levels. Steady-state *S*-palmitoylation analysis uses hydroxylamine-dependent thioester hydrolysis, thiol capture, and enrichment[15]. In the acyl-Resin-Assisted Capture (acyl-RAC) protocol, thiols are first reduced and alkylated, and hydroxylamine is added to hydrolyze thioesterified cysteines for capture on pyridyl-disulfide conjugated agarose resin. This method is agnostic to the nature of the acyl group and

captures both *S*-palmitoylated and endogenously thioesterified proteins, including lipoamide cofactor-dependent dehydrogenases and ubiquitin ligases.

Despite the prevalence of both bioorthogonal metabolic labeling and hydroxylamine-switch assays for *S*-palmitoylation, there has been little direct comparison. In the malaria parasite *P. falciparum*, about 57% of proteins were identified in both alkynyl fatty acid labeling and hydroxylamine switch enrichment and mass spectrometry analysis[16], which was greater than the 20% overlap observed in HeLa cells[17]. Here we find that hydroxylamine-switch methods are orders of magnitude more sensitive than alkynyl fatty acid bioorthogonal labeling (Figure 3a), which may explain the low fraction (~10%) of proteins that overlap between methods (Figure 3b). To our surprise, 17-ODYA labeling is almost undetectable in direct comparison to hydroxylamine-switch methods. This observation suggests a major reevaluation of many *S*-palmitoylation studies since each method may detect proteins with different properties. In addition, this demonstrates that either *S*-palmitoylation turnover is massively slower than previously widely accepted, or endogenous free fatty acid pools out compete 17-ODYA for incorporation into endogenous *S*-palmitoylation sites.

To explore this further, in-gel hydroxylamine-switch analysis reported no obvious changes in steady-state *S*-palmitoylation after HDFP or both HDFP and 17-ODYA (Figure 4a **and** Figure S4a). Analysis of HDFP or HDFP/17-ODYA treated cells by acyl-RAC enrichment and multiplexed mass spectrometry analysis confirmed that lipase inhibition has no major effect on global steady-state *S*-palmitoylation levels (Figures 4b, S4b, and Table S4–5). These results were corroborated by gel-based analysis of RAS and SCRIB, which were selected based on their validated dynamic *S*-palmitoylation[5, 8] and their rapid increase in 17-ODYA labeling after HDFP treatment. Following acyl-RAC enrichment, neither protein was significantly different in HDFP treated samples (Figures 4c-d and S4c-d). Clearly, metabolic labeling labels a dynamic subset of *S*-palmitoylated proteins, which appears much smaller than the total amount of the *S*-palmitoylated protein.

Conversely, the broadly reactive *S*-palmitoylation inhibitor 2-bromo-palmitate (2BP)[18] reduced both RAS and SCRIB steady-state *S*-palmitoylation, verifying sufficient sensitivity to measure chemically modulated *S*-palmitoylation. Nonetheless, 2BP can directly modify all known depalmitoylases, including APT[19] and ABHD17 enzyme families[18], and thus could affect both the *S*-palmitoylation and depalmitoylation arms of the *S*-palmitoylation cycle. Importantly, gel-based analysis using standard image auto-thresholds demonstrates an apparent increase in Ras *S*-palmitoylation (Figure S4d). After loading control normalization, these effects are neither large nor significant, underscoring the importance of biological replicates for accurate and precise measurements. Overall, this analysis demonstrates that while HDFP enhances the stoichiometry of alkynyl labeling, it does not greatly impact bulk steady-state *S*-palmitoylation levels in either 293T or HAP1 cells.

The protein depalmitoylases APT1 and APT2 are structurally similar α/β-hydrolases [20] and catalyze depalmitoylation across at least dozens of proteins either *in vitro* or in cells[6]. Despite the predicted broad role for APT1 and APT2 in protein depalmitoylation, cell-based studies exclusively rely on APT inhibitors or RNA interference to probe cellular phenotypes. Even with an arsenal of APT1 and APT2 inhibitors[21], there have not been any reported

efforts to profile APT1 and/or APT2 dependent *S*-palmitoylation. To address this gap, APT1 (*Lypla1*) and APT2 (*Lypla2*) knockout mice were acquired through commercial sources and crossed to generate double knockout mice. The resulting double knockout mice were viable and fertile, yet were born at sub-Mendelian frequencies. Whole brains were harvested from 3-month old APT1$^{-/-}$/APT2$^{-/-}$ mice for *S*-palmitoylation analysis. Double knockout was confirmed by fluorophosphonate activity-based profiling, which also demonstrates no obvious compensatory changes across abundant brain serine hydrolases, including the candidate depalmitoylase ABHD17A (Figure 5a). As observed with HDFP-treated cells, there was no visual change in the *S*-palmitoylation profile by in-gel hydroxylamine-switch analysis (Figure 5b). These observations were confirmed by multiplexed mass spectrometry, again reporting no obvious changes (up or down by 2-fold or more) in *S*-palmitoylation levels by APT1 and APT2 deletion, with the exception of MAP6 (2.2-fold increase) (Figure 5c and Table S6). Interestingly, MAP6 was recently reported to require ABHD17 activity to maintain a dynamic *S*-palmitoylation necessary for synaptic trafficking[22]. This suggests either an interplay between ABHD17 and APT enzymes or differential depalmitoylase regulation between cultured primary neurons and brain. Total MAP6 levels are increased in knockout tissue, suggesting APT1 and/or APT2 may destabilize MAP6 or reduce expression, potentially through regulating its *S*-palmitoylation. The dataset also highlights several proteins with reduced *S*-palmitoylation and/or expression, including the secreted growth hormone somatotropin (4-fold) and several proteins with proteins with Ca^{2+}-responsive C2 domains (copine-1/−6, PKCα/β/γ) and Ca^{2+}-dependent annexins (A5/A6/A7) (1.75 – 2.5-fold). In contrast to decades of over-expression studies in cultured cells, APT1 and APT2 knockout does not greatly affect steady-state *S*-palmitoylation levels in total mouse brain.

Discussion

S-palmitoylation is widely presented as a dynamic modification, yet due to technical challenges, there has been little progress towards profiling proteome-wide dynamics. Here we establish a method for temporal profiling and confirm a direct correlation between dynamic *S*-palmitoylation and the rate of fatty acid incorporation. We anticipate this multiplexed mass spectrometry approach will significantly impact the analysis of the *S*-palmitoylation cycle, including further annotation of select depalmitoylases, substrate assignment to zDHHC protein acyl transferases, and analysis of signal-dependent regulation. Since zDHHC enzymes often share common substrates[23], this approach could provide an opportunity to bypass steady-state compensatory effects and assign substrates based on kinetic signatures of fatty acid incorporation. Such analysis could be complicated by acyl-CoA substrate preferences among zDHHC enzymes[24], but provides a platform to profile incorporation of different alkynyl fatty acid derivatives across the proteome.

We recently demonstrated HDFP treatment redistributes G_{α}s randomly across internal membranes, independent of GPCR activation[4]. This corresponds similarly to analysis of NRAS random distribution after treatment with the promiscuous depalmitoylase inhibitor Palmostatin B[3]. Based on our comparative acyl-RAC and 17-ODYA profiling, we propose a model where depalmitoylase inhibition can affect the rate of *S*-palmitoylation, yet maintain relatively constant steady state *S*-palmitoylation levels. Accordingly, when the *S*-

palmitoylation cycle is stalled, the functional affect may not be a shift in steady-state *S*-acylation, but instead a release from the vesicular flux and random localization across internal membranes. Our data demonstrates that metabolic labeling approaches only access a limited fraction of the total *S*-palmitoylated protein, which diminishes any effects of depalmitoylase inhibition. Clearly the gel-based profile of labeled proteins is visually quite different between alkynyl fatty acid labeling and hydroxylamine-switch methods.

While HDFP treatment stimulates 17-ODYA incorporation, this increase only represents a minor fraction of the bulk *S*-palmitoylated form. While several studies have reported changes in *S*-palmitoylation of select targets by acyl-RAC after APT inhibition[6], these effects may be cell line dependent[5]. In addition, APT enzymes represent only a fraction of depalmitoylase activity in 293T cells, suggesting possible compensation from other uncharacterized enzymes[25]. While clarifying the HDFP-sensitive enzymes involved in this effect is ongoing, this compensation may be linked to ABHD17 family depalmitoylases[26, 27]. The development of potent and selective ABHD17 inhibitors will begin to address these questions, while avoiding technical challenges in deriving ABHD17A, ABHD17B, and ABHD17C triple knockout cells, particularly when knockout of individual members reduces cell viability across many cancer cell lines[28]. The data presented here suggests steady-state *S*-palmitoylation is not greatly affected by addition of bioorthogonal fatty acids, depalmitoylase inhibitors, or genetic deletion of depalmitoylases, whether or not they modulate acyl-CoA levels in cells.

APT enzymes have been studied nearly exclusively in cancer cell models, where APT1 and APT2 inhibition represses oncogenic signaling and stem cell-like features by modulating lateral polarity complexes[5] and asymmetric cell division[29]. Surprisingly, APT1$^{-/-}$/APT2$^{-/-}$ mice are viable and have no overt developmental defects. While detailed analysis of these mutant mice will require more focused effort, this analysis suggests APT enzymes exert their effects only in specific cell contexts[29, 30]. Since APT1$^{-/-}$/APT2$^{-/-}$ mice have no measureable changes in steady-state *S*-palmitoylation, it is unclear how relevant these enzymes are to regulating *S*-palmitoylation dynamics over other lipid hydrolase activities[31]. Future studies are essential to reveal potential compensatory mechanisms and any *in vivo* functional role for these protein depalmitoylases.

Overall, the methods and analyses presented reveal the kinetic profile of *S*-palmitoylation in cells, revealing new insights to proteins linked to dynamic *S*-palmitoylation cycles. These methods reveal potential limitations of steady-state analysis while presenting new opportunities for temporal profiling of *S*-palmitoylation.

Methods

Cell Culture.

Human 293T cells were cultured in Dulbecco's Modified Eagle Media (DMEM / Invitrogen) supplemented with 1% (v / v) 10000 Units / mL penicillin-streptomycin (Invitrogen), 4.5 g / L D-Glucose, 2 mM L-Glutamine, 110 mg / L sodium pyruvate, and 10% (v / v) dialyzed fetal bovine serum (JR Scientific). HAP1 cells were cultured in Iscove′s Modified Dulbecco ′s Medium (IMDM / Invitrogen) supplemented with 1% (v / v) 10000 Units / mL penicillin-

streptomycin, and 10 % (v / v) dialyzed fetal bovine serum. Jurkat cells were grown in Roswell Park Memorial Institute (RPMI) 1640 (Invitrogen) supplemented with 2.38 g / L HEPES buffer, 1.5 g / L sodium bicarbonate, 1 % (v / v) 10000 Units / mL penicillin-streptomycin, 4.5 g / L D-glucose, 2 mM L-Glutamine, 110 mg / L sodium pyruvate, and 5 % (v / v) dialyzed fetal bovine serum. There was no additional effort to authenticate these cell lines, since the morphological characteristics matched signatures for each cell line.

Metabolic labeling and inhibitor treatments.

17-ODYA labeling was performed as described previously [8]. HDFP, ML348, and ML349 syntheses were previously reported[8, 20]. Other inhibitors were purchased from Sigma (2-bromohexadecanoic acid, TVB-3166, and ABC44) or Cayman (JW480, WWL229, and WWL70). At ~90 % confluency, the growth media was aspirated and new media containing the inhibitor was added to the cells (Control = 0.1% v / v DMSO final). For ABPP and acyl-RAC proteomic experiments, cells were incubated with HDFP for 3 hours. After incubation, 20 μM 17-ODYA (Cayman) was added. At different time points, cells were washed with cold DPBS (Invitrogen) and scraped off the plate. The cell pellets were washed with DPBS and stored at −80 °C.

17-ODYA click chemistry and enrichment.

17-ODYA detection in cell homogenates was performed as previously described[8, 20]. Frozen cell-pellets were resuspended in DPBS and lysed by sonication. For in-gel fluorescence analysis, 50 μg of protein (quantified using the BCA protein assay kit; Bio-Rad) was incubated with 1 mM tris(2-carboxyethyl)phosphine (TCEP;Sigma), 20 μM TAMRA azide (Click Chemistry Tools), 1 mM $CuSO_4$, and 100 μM Tris((1-benzyl-1H-1,2,3-triazol-4-yl)methyl)amine (TBTA; Cayman) for 1 hour at room temperature. The samples were resolved by 12 % SDS-PAGE (180 V;1 hr) and imaged using Azure C600 (Azure Biosystems). Samples prepared for mass spectrometry analysis included 1 biological replicate per time point (palmitic acid as time 0) for each condition (DMSO or 1 μM HDFP). The sonicated homogenate was separated into soluble (S100) and insoluble (P100) fractions by ultracentrifugation at 100,000g for 45 min. 1 mg of the P100 fraction was incubated with the click chemistry reagents listed above, except Biotin PEG3 Azide (500 μM; Click Chemistry Tools) was substituted for TAMRA azide. After 1 hour, proteins were extracted with methanol and chloroform (4 eq. aqueous, 4 eq. methanol, 1 eq. chloroform). The insoluble pellet was washed with methanol and resuspended in 6 M urea / 2% SDS in PBS. Protein concentrations normalized again across all samples. Samples were then incubated with 5 mM TCEP (pH 7) for 30 min, followed by addition of 20 mM iodoacetamide for 1 hour in dark. The samples were diluted 3-fold and the same amount of protein was added to 75 μL of pre-washed Streptavidin beads (Thermo) for 90 minutes. The beads were washed 5 times with PBS containing 2 M urea and 0.2 % SDS and 5 more times in PBS. Finally, the beads were resuspended in 100 μL of 50 mM triethylammonium bicarbonate (TEAB) and 1.3 μg of mass spectrometry-grade Trypsin/Lys C mix (Promega). After overnight digestion at 37°C, the eluted peptides were incubated with TMT 6plex (Thermo) reagents according to the manufacturer's protocols. The samples were mixed into 1 tube, desalted with an Oasis PRIME HLB μElution Plate (Waters), dried using a Thermo Savant SpeedVac, and stored at −80 °C.

Serine Hydrolase Activity-based Profiling.

Cells were incubated with inhibitors in culture, and then scaped and lysed by sonication. For fluorescent gel-based analysis, 50 μg of protein was incubated with 2 μM fluorophosphonate (FP)-TAMRA[32] for 30 minutes. For the proteomic analysis, 4 biological replicates per condition (20 μM HDFP, 1 μM HDFP, DMSO) were used and 2 of each condition was combined into 1 TMT 6plex run. 1 mg of whole cell lysate was incubated with 5 μM FP-biotin for 1 hour at room temperature. The streptavidin enrichment and mass spectrometry sample preparation procedures are identical to the 17-ODYA enrichment sample preparation.

Acyl-RAC.

Cell pellets were resuspended in Buffer 1 (50 mM HEPES pH 7.4, 1 mM EDTA, 100 mM NaCl), sonicated, and fractionated by centrifugation at 100,000g for 45 minutes at 4 °C. The insoluble fraction was resuspended in Buffer 2 (50 mM HEPES pH 7.4, 2 % SDS) and quantified with BCA protein assay kit. 1–2 mg of protein was diluted in 1 mL of Buffer 3 (50 mM HEPES pH 7.4, 6 M urea, 1 mM EDTA, 2 % SDS) and incubated with 10 mM TCEP for 30 minutes at room temperature, followed by 50 mM iodoacetamide for 1 hour in dark. The proteins were precipitated by chloroform / methanol extraction (as above) and resuspended in Buffer 2 and re-quantified. For the hydroxylamine-switch gel-based analysis, 0.5 M neutralized hydroxylamine was added to each sample and incubated for 15 minutes, followed by 1 μM tetramethylrhodamine-5-Iodoacetamide Dihydroiodide (5-TMRIA (noted IAM-TAMRA); Thermo) for 30 minutes. For the enrichment analysis, the reduced and alkylated proteins (>1 mg) were added to the 100 μL of water-activated, pre-washed Thiopropyl-Sepharose 6B beads (Sigma) in Buffer 3, followed by the addition of 0.5 M hydroxylamine. The samples were incubated for 2 hours at room temperature and washed 5 times with Buffer 2 and washed 5 more times in 50 mM HEPES. For the western-blot analysis, beads were resuspended in the 1X loading buffer (10% glycerol, 62.5 mM tris pH 6.8, 1% 2-mercaptoethanol, 0.05% bromophenol blue, and 1% SDS) and heated for 5 minutes at 90 °C. The supernatant analyzed by SDS-PAGE. For the proteomic analysis, 4 biological replicates per condition (DMSO, +HDFP, +HDFP&17-ODYA) were used. Two of each condition were combined into one TMT 6plex run. The beads were resuspended in 50 mM TEAB and incubated with Trypsin/Lys C mix (Promega) at 37°C overnight. The supernatants were TMT labeled and desalted as above. For the mouse brain samples, 3 experimental replicates per condition (WT or APTs KO) was combined into one TMT 6plex run. Tissue was washed in Buffer 1, then dounce homogenized at 4°C. The lysate was briefly centrifuged at 1000*g* for 5 minutes to remove debris, fractionated and processed for the proteomic sample preparation as above.

Western blotting.

Gels were transferred to methanol-activated Immobilon-FL membrane (Millipore) in the transfer buffer (25 mM Tris-base,192 mM glycine, 10 % methanol) at 75 V for 2 hours. Proteins were probed with anti-alpha tubulin (1:1000; Sigma #T6074), anti-APT1 (1:500; Millipore; #MABS166), anti-APT2 (1:500; Thermo; #PA-527653), anti-Pan Ras (1:1000; Millipore; #05–516), anti-Scrib (1:1000; Millipore; #MAB1820), anti-MAP6 (1:1000; anti-STOP; Cell Signaling Technology; #4265), or anti-ABHD17A (1:1000; Aviva Systems

Biology; #ARP67573_P050) for 16 hours at 4°C and then incubated with secondary anti-mouse or anti-rabbit horseradish peroxidase (HRP;1:1000; Thermo; #32430) for 1 hour at room temperature. Blots were developed by West Pico Chemiluminescent Substrate (Thermo) and then the chemiluminescence was detected by Azure c600 imager (Azure Biosystems).

Knockout Mice.

Lypla1 (APT1) knockout mice were generated by purchasing the cryopreserved TF1704 model from Taconic Biosciences. C57BL/6NTac females were impregnated with cryopreserved sperm from a mixed C57BL/6–129/SvEv background harboring a gene-trap ("gt") cassette between Lypla1 exons 2 and 3. After intercrossing, western blot and gel- and mass-spec-based experiments with FP probes confirmed complete loss of APT1 protein in $Lypla1^{gt/gt}$ mice. Lypla2 (APT2) knockout mice were generated by acquiring cryopreserved sperm from the KOMP repository at UC Davis harboring the $Lypla2^{tm1a(KOMP)Mbp}$ "knockout-first" gene-trap cassette which was inserted between exons Lypla2 1 and 2. Homozygous $Lypla2^{gt/gt}$ mice were found to retain ~20% residual APT2 expression via gel- and mass-spec-based experiments with FP-probes. Complete ablation of APT2 protein was achieved by crossing $Lypla2^{gt/gt}$ mice with a C757BL/6 mouse line with ubiquitous expression of Cre recombinase (Taconic #12524) which resulted in removal of Lypla2 exons 2–10 from the genome. The resulting $Lypla2^{Cre/Cre}$ mice were confirmed to have no residual APT2 protein expression, as measured by gel- and mass-spec based experiments with FP probes. Lypla1/Lypla2 (APT1/APT2) double knockout mice were generated by crossing $Lypla1^{gt/gt}$ mice with $Lypla2^{gt/gt}$ mice. The resulting $Lypla1^{gt/gt}$;$Lypla2^{gt/gt}$ mice were then crossed with a ubiquitous Cre deleter line (Taconic #12524) to accomplish removal of Lypla2 exons 2–10 and complete ablation of APT2 expression.

Supplementary Material

Refer to Web version on PubMed Central for supplementary material.

Acknowledgements

We would like to thank Abide Therapeutics for generously providing $APT1^{-/-}$/$APT2^{-/-}$ mouse tissues, G. van der Goot (EPFL) for providing HAP1 cells, V. Basrur (University of Michigan) for assistance with mass spectrometry, and S. Haynes (University of Michigan) for bioinformatics support. Financial support was provided by the National Institutes of Health DP2 GM114848 and the University of Michigan.

References

[1]. Rocks O, Gerauer M, Vartak N, Koch S, Huang ZP, Pechlivanis M, Kuhlmann J, Brunsveld L, Chandra A, Ellinger B, Waldmann H, and Bastiaens PI (2010) The palmitoylation machinery is a spatially organizing system for peripheral membrane proteins, Cell 141, 458–471. [PubMed: 20416930]

[2]. Schmick M, Kraemer A, and Bastiaens PI (2015) Ras moves to stay in place, Trends Cell Biol 25, 190–197. [PubMed: 25759176]

[3]. Dekker FJ, Rocks O, Vartak N, Menninger S, Hedberg C, Balamurugan R, Wetzel S, Renner S, Gerauer M, Scholermann B, Rusch M, Kramer JW, Rauh D, Coates GW, Brunsveld L, Bastiaens PI, and Waldmann H (2010) Small-molecule inhibition of APT1 affects Ras localization and signaling, Nat. Chem. Biol 6, 449–456. [PubMed: 20418879]

[4]. Martin BR, and Lambert NA (2016) Activated G Protein Galphas Samples Multiple Endomembrane Compartments, J. Biol. Chem 291, 20295–20302. [PubMed: 27528603]

[5]. Hernandez JL, Davda D, Cheung See Kit M, Majmudar JD, Won SJ, Gang M, Pasupuleti SC, Choi AI, Bartkowiak CM, and Martin BR (2017) APT2 Inhibition Restores Scribble Localization and S-Palmitoylation in Snail-Transformed Cells, Cell Chem. Biol 24, 87–97. [PubMed: 28065656]

[6]. Won SJ, Cheung See Kit M, and Martin BR (2018) Protein depalmitoylases, Crit. Rev. Biochem. Mol. Biol 53, 83–98. [PubMed: 29239216]

[7]. Gao X, and Hannoush RN (2018) A Decade of Click Chemistry in Protein Palmitoylation: Impact on Discovery and New Biology, Cell Chem Biol 25, 236–246. [PubMed: 29290622]

[8]. Martin BR, Wang C, Adibekian A, Tully SE, and Cravatt BF (2011) Global profiling of dynamic protein palmitoylation, Nat Methods 9, 84–89. [PubMed: 22056678]

[9]. Thiele C, Papan C, Hoelper D, Kusserow K, Gaebler A, Schoene M, Piotrowitz K, Lohmann D, Spandl J, Stevanovic A, Shevchenko A, and Kuerschner L (2012) Tracing fatty acid metabolism by click chemistry, ACS Chem. Biol 7, 2004–2011. [PubMed: 22999348]

[10]. McAlister GC, Nusinow DP, Jedrychowski MP, Wuhr M, Huttlin EL, Erickson BK, Rad R, Haas W, and Gygi SP (2014) MultiNotch MS3 enables accurate, sensitive, and multiplexed detection of differential expression across cancer cell line proteomes, Anal. Chem 86, 7150–7158. [PubMed: 24927332]

[11]. McMichael TM, Zhang L, Chemudupati M, Hach JC, Kenney AD, Hang HC, and Yount JS (2017) The palmitoyltransferase ZDHHC20 enhances interferon-induced transmembrane protein 3 (IFITM3) palmitoylation and antiviral activity, J Biol Chem 292, 21517–21526. [PubMed: 29079573]

[12]. Abrami L, Dallavilla T, Sandoz PA, Demir M, Kunz B, Savoglidis G, Hatzimanikatis V, and van der Goot FG (2017) Identification and dynamics of the human ZDHHC16-ZDHHC6 palmitoylation cascade, Elife 6.

[13]. Blanc M, David F, Abrami L, Migliozzi D, Armand F, B¸rgi J, and van der Goot F (2015) SwissPalm: Protein Palmitoylation database [version 1; referees: 3 approved], Vol. 4.

[14]. Zhang J, Huang Y, Chen J, Zhu H, and Whiteheart SW (2018) Dynamic cycling of t-SNARE acylation regulates platelet exocytosis, J Biol Chem 293, 3593–3606. [PubMed: 29352103]

[15]. Forrester MT, Hess DT, Thompson JW, Hultman R, Moseley MA, Stamler JS, and Casey PJ (2011) Site-specific analysis of protein S-acylation by resin-assisted capture, J. Lipid. Res 52, 393–398. [PubMed: 21044946]

[16]. Jones ML, Collins MO, Goulding D, Choudhary JS, and Rayner JC (2012) Analysis of protein palmitoylation reveals a pervasive role in Plasmodium development and pathogenesis, Cell Host Microbe 12, 246–258. [PubMed: 22901544]

[17]. Thinon E, Fernandez JP, Molina H, and Hang HC (2018) Selective Enrichment and Direct Analysis of Protein S-Palmitoylation Sites, J Proteome Res 17, 1907–1922. [PubMed: 29575903]

[18]. Davda D, El Azzouny MA, Tom CT, Hernandez JL, Majmudar JD, Kennedy RT, and Martin BR (2013) Profiling targets of the irreversible palmitoylation inhibitor 2-bromopalmitate, ACS Chem. Biol 8, 1912–1917. [PubMed: 23844586]

[19]. Pedro MP, Vilcaes AA, Tomatis VM, Oliveira RG, Gomez GA, and Daniotti JL (2013) 2-Bromopalmitate reduces protein deacylation by inhibition of acyl-protein thioesterase enzymatic activities, PLoS One 8, e75232. [PubMed: 24098372]

[20]. Won SJ, Davda D, Labby KJ, Hwang SY, Pricer R, Majmudar JD, Armacost KA, Rodriguez LA, Rodriguez CL, Chong FS, Torossian KA, Palakurthi J, Hur ES, Meagher JL, Brooks CL, 3rd, Stuckey JA, and Martin BR (2016) Molecular Mechanism for Isoform-Selective Inhibition of Acyl Protein Thioesterases 1 and 2 (APT1 and APT2), ACS Chem Biol 11, 3374–3382. [PubMed: 27748579]

[21]. Davda D, and Martin BR (2014) Acyl protein thioesterase inhibitors as probes of dynamic S-palmitoylation, Med. Chem. Comm 5, 268–276.

[22]. Tortosa E, Adolfs Y, Fukata M, Pasterkamp RJ, Kapitein LC, and Hoogenraad CC (2017) Dynamic Palmitoylation Targets MAP6 to the Axon to Promote Microtubule Stabilization during Neuronal Polarization, Neuron 94, 809–825 e807. [PubMed: 28521134]

[23]. Lemonidis K, Salaun C, Kouskou M, Diez-Ardanuy C, Chamberlain LH, and Greaves J (2017) Substrate selectivity in the zDHHC family of S-acyltransferases, Biochem. Soc. Trans 45, 751–758. [PubMed: 28620036]

[24]. Greaves J, Munro KR, Davidson SC, Riviere M, Wojno J, Smith TK, Tomkinson NC, and Chamberlain LH (2017) Molecular basis of fatty acid selectivity in the zDHHC family of S-acyltransferases revealed by click chemistry, Proc. Natl. Acad. Sci. U. S. A 114, E1365–E1374. [PubMed: 28167757]

[25]. Kathayat RS, Elvira PD, and Dickinson BC (2017) A fluorescent probe for cysteine depalmitoylation reveals dynamic APT signaling, Nat. Chem. Biol 13, 150–152. [PubMed: 27992880]

[26]. Yokoi N, Fukata Y, Sekiya A, Murakami T, Kobayashi K, and Fukata M (2016) Identification of PSD-95 Depalmitoylating Enzymes, J Neurosci 36, 6431–6444. [PubMed: 27307232]

[27]. Lin DT, and Conibear E (2015) ABHD17 proteins are novel protein depalmitoylases that regulate N-Ras palmitate turnover and subcellular localization, Elife 4, e11306. [PubMed: 26701913]

[28]. Wang T, Yu H, Hughes NW, Liu B, Kendirli A, Klein K, Chen WW, Lander ES, and Sabatini DM (2017) Gene Essentiality Profiling Reveals Gene Networks and Synthetic Lethal Interactions with Oncogenic Ras, Cell 168, 890–903 e815. [PubMed: 28162770]

[29]. Stypulkowski E, Asangani IA, and Witze ES (2018) The depalmitoylase APT1 directs the asymmetric partitioning of Notch and Wnt signaling during cell division, Sci. Signal 11.

[30]. Hernandez JL, Davda D, Majmudar JD, Won SJ, Prakash A, Choi AI, and Martin BR (2016) Correlated S-palmitoylation profiling of Snail-induced epithelial to mesenchymal transition, Mol. Biosyst 12, 1799–1808. [PubMed: 27030425]

[31]. Manna JD, Wepy JA, Hsu KL, Chang JW, Cravatt BF, and Marnett LJ (2014) Identification of the major prostaglandin glycerol ester hydrolase in human cancer cells, J. Biol. Chem 289, 33741–33753. [PubMed: 25301951]

[32]. Xu H, Majmudar JD, Davda D, Ghanakota P, Kim KH, Carlson HA, Showalter HD, Martin BR, and Amidon GL (2015) Substrate-Competitive Activity-Based Profiling of Ester Prodrug Activating Enzymes, Mol. Pharmaceutics 12, 3399–3407.

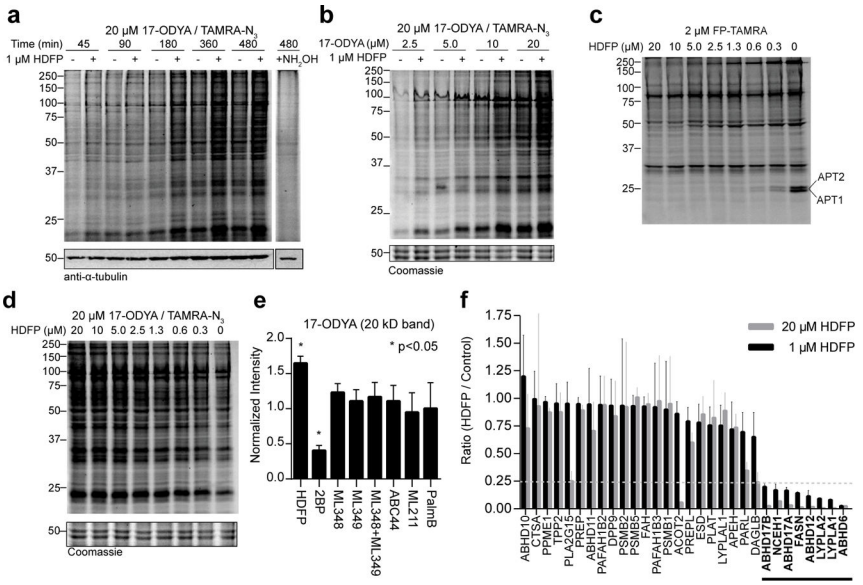

Figure 1. Depalmitoylase inhibition enhances 17-ODYA labeling.

(a) HDFP enhances 17-ODYA incorporation at all time points during labeling. Neutralized 0.5 M hydroxylamine (NH_2OH) hydrolyzes 17-ODYA labeling, demonstrating the presence of a thioester linkage. (b) Different concentrations of 17-ODYA do not affect HDFP-dependent enhanced probe incorporation. (c) Fluorophosphonate-TAMRA (FP-TAMRA) competitive ABPP demonstrates APT enzymes are inactivated by sub-micromolar HDFP concentrations. (d) Dose-dependent profile of HDFP-dependent enhancement of 17-ODYA incorporation. (e) APT inhibition does not affect 17-ODYA incorporation levels in 293T cells. 1 μM HDFP, 50 μM 2BP, 10 μM ML348, ML349, and PalmB, 1 μM ABC44 and ML211 were used. Data represents the average intensity of the ~20 kD band (encompassing Ras small GTPases) in biological replicates (N = 3, standard error) of 17-ODYA gels, shown in Figure S2b. (f) Competitive ABPP mass spectrometry analysis of HDFP inhibition across the serine hydrolase family. Error bars represent error propagated from standard errors at differing HDFP concentrations, quantified from multiplexed TMT isobaric reporter ions. N = 4. Serine hydrolases with >2 PSMs are shown. All experiments were performed in human 293T cells.

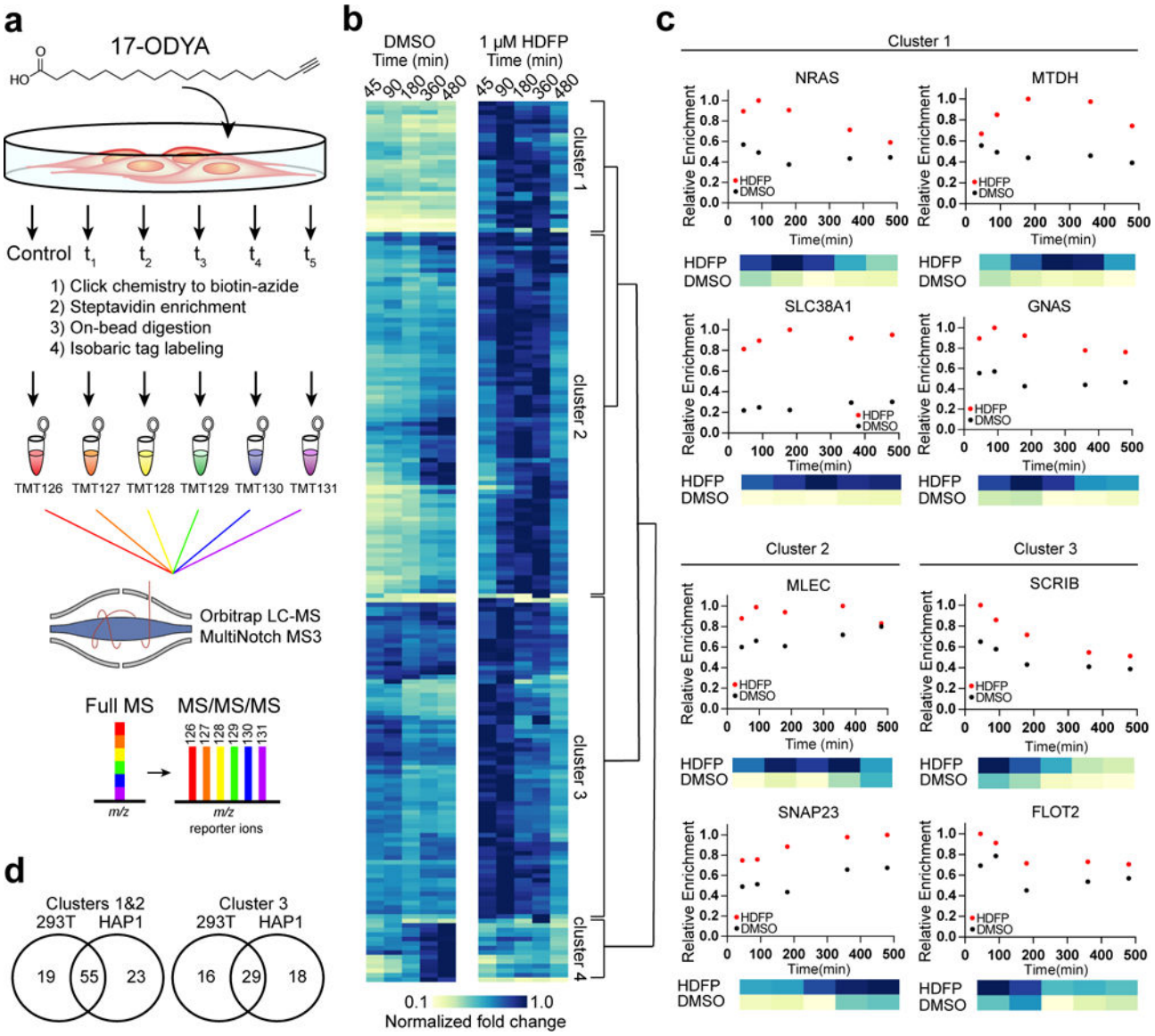

Figure 2. Time-dependent profiling of 17-ODYA incorporation identifies kinetic clusters of dynamic *S*-palmitoylated proteins.

(a) Schematic of bioorthogonal temporal *S*-palmitoylation profiling by multiplexed quantitative mass spectrometry. (b) Hierarchical clustering of 17-ODYA enriched *S*-palmitoylated proteins across both control and 1 μM HDFP-treated cells reveals distinct kinetic clusters in 293T cells. Proteins with >2-fold enrichment and at least 3 PSMs are shown. The heat map is normalized to the highest point along the labeling time course. Branches were simplified to highlight higher level grouping. (c) Representative labeling time course of select proteins from each subclass. Unique peptides were used to confirm analysis of RhoA and not RhoB, as both are frequently annotated *S*-palmitoylated proteins[13]. (d) Conserved kinetic profiles of temporal *S*-palmitoylation between human 293T and HAP1 cells (Figure S3).

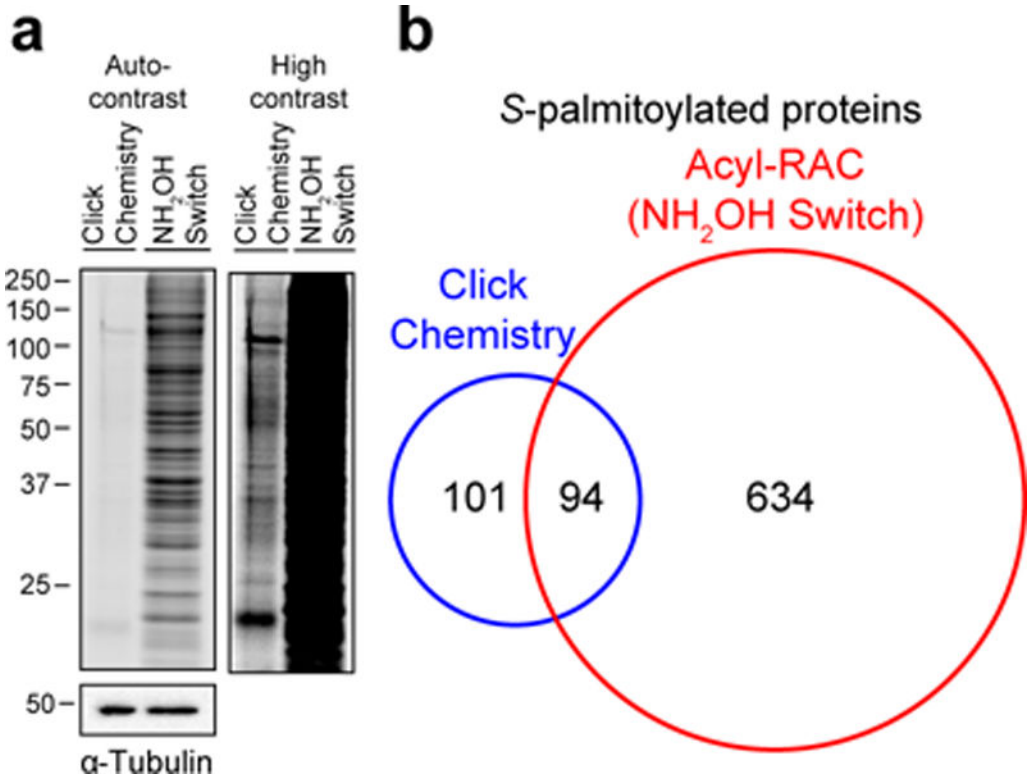

Figure 3. Comparison of 17-ODYA and acyl-RAC enrichment of *S*-palmitoylated proteins.

(A) Gel-based analysis of alkynyl fatty acid metabolic labeling and cli9+ck chemistry detection of *S*-palmitoylation compared to hydroxylamine-switch analysis by iodoacetamide-TAMRA detection. (B) Limited overlap of click chemistry and acyl-RAC analysis of specifically enriched S-palmitoylated proteins from 293T cells. Mass spectrometry data is reported in Tables S2 and S4.

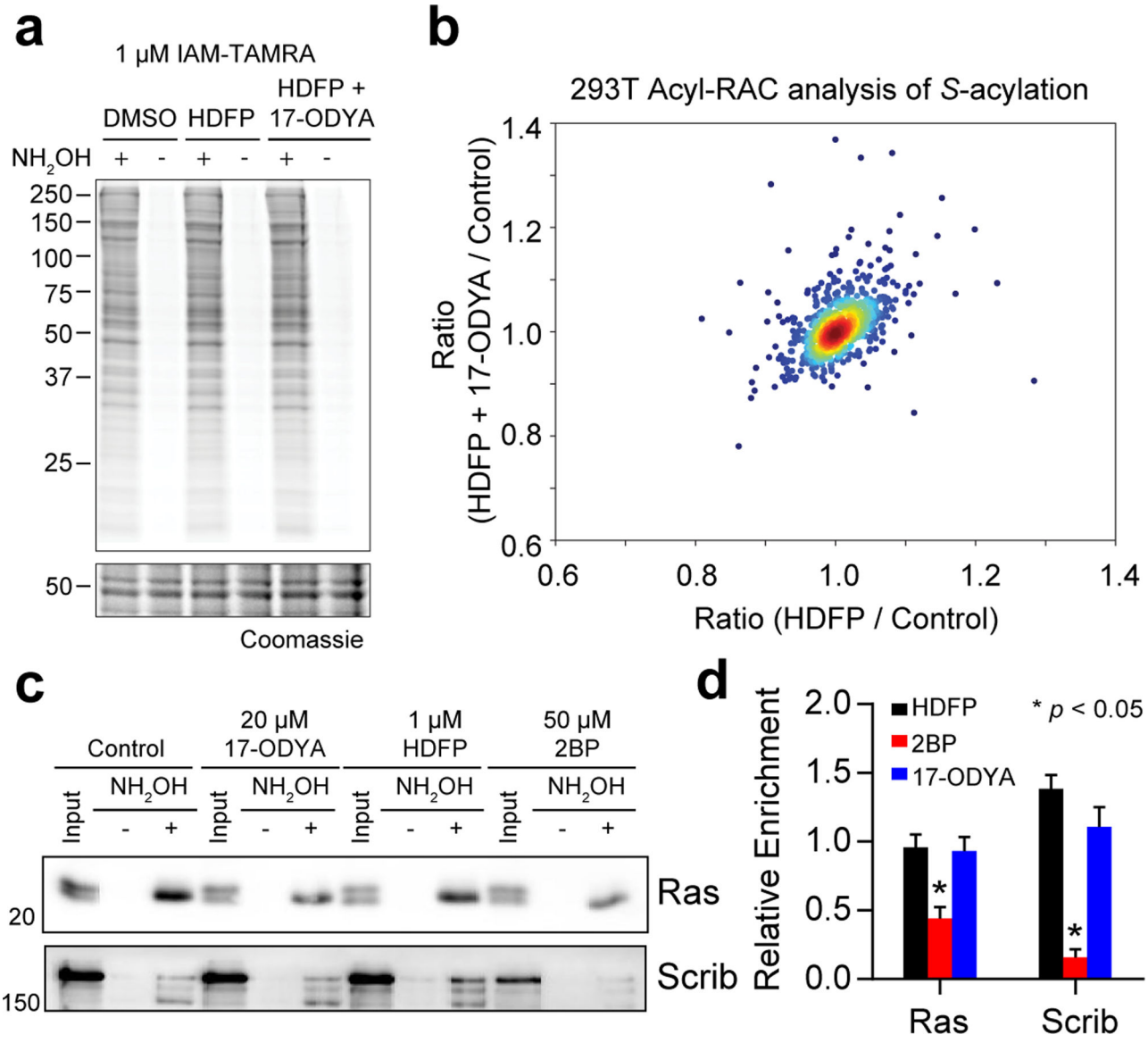

Figure 4. Depalmitoylase inhibition does not influence steady-state *S*-palmitoylation.

(a) In-gel analysis of *S*-palmitoylation using the hydroxylamine-switch analysis reports equivalent labeling profiles after 17-ODYA and HDFP treatment. Iodoacetamide-rhodamine (IAM-TAMRA) labeling reports the presence of hydroxylamine sensitive thiols. (b) Equivalent enrichment of *S*-palmitoylated proteins by quantitative proteomic analysis of acyl-RAC enriched proteins from control (DMSO) and HDFP (1 μM) or HDFP (1 μM) +17-ODYA (20 μM) treated cells, N=4. Proteins with >2 PSMs, multiple annotations in SwissPalm are shown. (c) Confirmatory acyl-RAC analysis of pan-RAS and SCRIB *S*-palmitoylation. (d) Quantitation of acyl-RAC enrichment relative to control (DMSO) across replicates after normalizing to input (Ras, N = 5 for all conditions except 17-ODYA, N = 3; Scrib, N = 3 for all conditions except 17-ODYA, N = 2, ±SEM) demonstrates no significant changes following HDFP treatment, but shows major reductions after 2BP treatment (two-tailed Student's t-test with unequal variance).

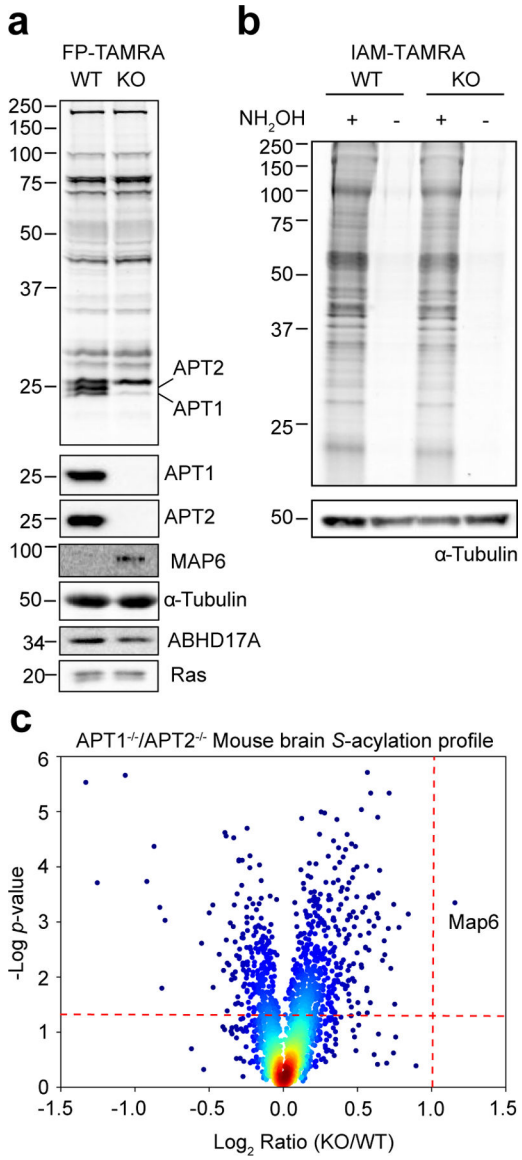

Figure 5. Steady-state *S*-palmitoylation is unaffected in APT1$^{-/-}$/APT2$^{-/-}$ mouse brains.

(a) FP-TAMRA labeling of active serine hydrolases in whole mouse brain homogenates confirms selective deletion of APT1 and APT2 with no observable compensatory changes across other hydrolases. Knockout was also confirmed by western blot. Labeling is shown with 2 μM FP-TAMRA. (b) Hydroxylamine-switch analysis of *S*-palmitoylation in normal and knockout samples does not reveal major changes in S-acylation profiles. Detection with 1 μM IAM-TAMRA. (c) Volcano plot analysis of acyl-RAC enrichment and multiplexed TMT mass spectrometry analysis of APT1$^{-/-}$/APT2$^{-/-}$ whole mouse brain homogenates (N=3). Red lines represent $p < 0.05$ from two-tailed Student's t-test with unequal variance (horizontal) and 2-fold change (vertical).